

Seismic performance evaluation of a three-dimensional unsymmetrical reinforced concrete building

Hyun-Kyu Lim^{1a}, Jun Won Kang^{*1}, Young-Geun Lee^{2b} and Ho-Seok Chi^{2c}

¹*Department of Civil Engineering, Hongik University, 94 Wausan-ro, Mapo-gu, Seoul 121-791, Republic of Korea*

²*Department of Structural System & Site Safety Evaluation, Korea Institute of Nuclear Safety, 62 Gwahak-ro, Yuseong-gu, Daejeon 305-338, Republic of Korea*

(Received May 1, 2015, Revised October 19, 2015, Accepted November 12, 2015)

Abstract. Reinforced concrete (RC) structures require advanced analysis techniques for better estimation of their seismic responses, especially in the case of exhibiting complex three-dimensional coupling of torsional and flexural behaviors. This study focuses on validating a numerical approach for evaluating the seismic response of a three-dimensional unsymmetrical RC structure through the participation in the SMART 2013 international benchmark program. The benchmark program provides material properties, detailed drawings of the RC structure, and input ground motions for the seismic response evaluation. In this study, nonlinear constitutive models of concrete and rebar were formed and local tests were conducted to verify the constitutive models in finite element analysis. Elastic calibration of the finite element model of the SMART 2013 RC structure was performed by comparing numerical and experimental results in modal and linear time history analyses. Using the calibrated model, nonlinear earthquake analysis and seismic fragility analysis were performed to estimate the behavior and vulnerability of the RC structure with various ground motions.

Keywords: reinforced concrete structure; time history analysis; seismic vulnerability assessment; SMART 2013 benchmark program

1. Introduction

Protection of critical civil infrastructure such as nuclear energy facilities and power stations from earthquakes has become a critical issue after recent disastrous events such as Christchurch and Fukushima earthquakes in 2011. To assess the damage of such structures due to earthquake, highly reliable analysis methods for evaluating seismic behavior and vulnerability of structures are needed (Bisch and Coin 1994, 1998, Kwak and Kim 2000, 2003, Lee *et al.* 2007). In particular, reinforced concrete (RC) structures require advanced analysis techniques for better estimation

*Corresponding author, Assistant Professor, E-mail: jwkang@hongik.ac.kr

^aGraduate Research Assistant, E-mail: limkuy11@gmail.com

^bSenior Researcher, E-mail: esdras1981@gmail.com

^cSenior Researcher, E-mail: hsc@kins.re.kr

of their seismic responses, especially in the case of exhibiting complex three-dimensional coupling of torsional and flexural behaviors (Juster-Lermitte *et al.* 2009, Crijanovschi *et al.* 2012). This study focuses on validating a numerical approach for evaluating the seismic response of a three-dimensional unsymmetrical RC structure through the participation in the SMART 2013 international benchmark program.

The benchmark program provides material properties, detailed drawings of the RC structure, and input ground motions for the seismic response evaluation (Richard and Chaudat 2014, Richard *et al.* 2014). In this study, nonlinear constitutive models of concrete and rebar were formed and local tests were conducted to verify the constitutive models in finite element analysis. Elastic calibration of the finite element model of the SMART 2013 RC structure was performed by comparing numerical and experimental results in modal and linear time history analyses. Using the calibrated model, nonlinear earthquake analysis and seismic fragility analysis were performed to estimate the behavior and vulnerability of the RC structure with various ground motions.

2. Modeling of the SMART 2013 mock-up structure

2.1 Material models for concrete and rebar

For the nonlinear seismic analysis of RC structures, it is important to establish constitutive models of concrete and rebar to capture realistic stress-strain behaviors during earthquake. There have been a lot of developments so far to make constitutive models capable of predicting the inelastic stress-strain behavior of concrete (Wang and Hsu 2001, Kwon and Spacone 2002, Shekarbeigi and Sharafi 2015). Table 1 summarizes representative mechanical properties of concrete and reinforcing steel provided by the SMART 2013 benchmark program (Richard and Chaudat 2014). With this information, we constructed a multilinear isotropic hardening model for

Table 1 Material properties for concrete and steel reinforcement

Material properties	Concrete	Rebar
Young's modulus (MPa)	32,000	210,000
Poisson ratio	0.2	0.3
Compressive strength (MPa)	30	500
Tensile strength (MPa)	2.4	500
Density (kg/m ³)	2,300	7,800

Table 2 Stress-strain data for multilinear isotropic hardening model of concrete

Stress (MPa)	Strain (mm/mm)
0.00	0.00000
9.00	0.00028
19.23	0.00108
25.95	0.00148
29.18	0.00187
30.00	0.00300

concrete based on a constitutive model discussed by Kachlakev and Miller (2001), as shown in Table 2. For steel reinforcement, we used an elastic-perfectly plastic model. Both constitutive models were incorporated in the finite element modeling of the SMART 2013 structure. ANSYS, a commercial finite element analysis package, was used for the modeling and analysis. The concrete material model is composed of five linear segments with the modulus decreasing successively from 32,000 MPa to nearly zero with respect to strain. The compressive strength of concrete is 30 MPa and its tensile strength is 2.4MPa. The yield stress of steel reinforcement is 500 MPa in both tension and compression at the strain of 0.00237.

2.2 Local tests

Local mechanical tests on a representative volume element (RVE) were performed to check if the constitutive models work properly in the finite element analysis. The steel and concrete RVEs are cubic elements with the side length of 1 m (Richard and Ragueneau 2012, 2013). The local test is composed of a series of uniaxial monotonic and cyclic tension compression tests on concrete and steel RVEs, as described in Table 3.

Figs. 1(a) and 1(b) show the stress-strain responses of concrete RVE under monotonic tension and compression loadings, respectively. The concrete RVE failed at the tensile stress of 2.4 MPa, while sustaining the maximum compressive stress of 30 MPa, as dictated by the constitutive model of concrete. Fig. 1(c) represents the stress-strain response of steel obtained from uniaxial cyclic tension and compression tests on the steel RVE. The hysteresis behavior captures the characteristics of the biaxial material model of steel effectively. Fig. 1(d) shows the hysteresis response of reinforced concrete RVE under uniaxial cyclic tension and compression loading with the displacement ranging from -4 mm to 1.5 mm. From the above local tests, it was demonstrated that the nonlinear material models of concrete and steel worked effectively in finite element analysis.

2.3 Finite element models for structural components

The SMART 2013 RC structure was built as a typical nuclear facility building with 1/4 scale of prototype structure, as shown in Fig. 2(a). The structural model consists of 7 parts (foundation, wall, slab, beam, column, rebar and shaking table). Rebar was modeled with the BEAM188

Table 3 Description of local tests

Test No.	Material	Aim	Loading Conditions
c.1	Concrete	Identify axial tension response of the concrete RVE	Uniaxial monotonic tension loading with the displacement ranging from 0 to 1 mm
c.2	Concrete	Identify axial compression response of the concrete RVE	Uniaxial monotonic compression loading with the displacement ranging from 0 to -10 mm
s.1	Steel	Identify axial cyclic response of the steel RVE	Uniaxial cyclic tension/compression loading with the displacement ranging from -10 mm to 10 mm
rc.1	Reinforced concrete	Identify axial cyclic response of the RC RVE	Uniaxial cyclic tension/compression loading with the displacement ranging from -4 mm to 1.5 mm

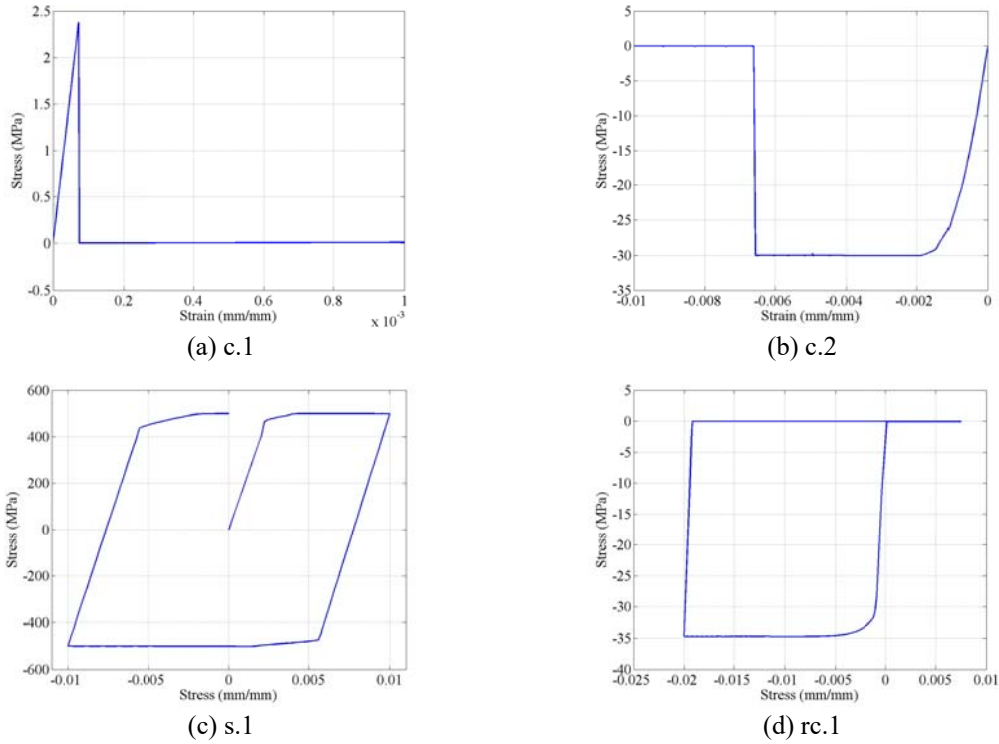
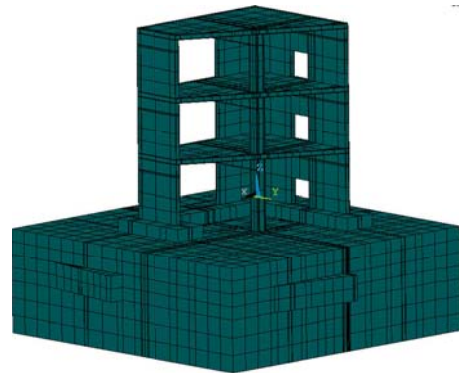


Fig. 1 Stress-strain responses from the local tests



(a) SMART 2013 RC structure



(b) Finite element model

Fig. 2 SMART 2013 mock-up structure for benchmark analysis

element, a three-dimensional beam element of ANSYS. The other 6 parts were modeled with the SOLID65 element, an 8-node brick element that can be used for modeling concrete in ANSYS. To ensure the behavior of concrete and rebar, the concrete elements shared the same nodes with rebar elements. Shown in Fig. 2(b) is the entire finite element model of the SMART 2013 structure including the shaking table.

3. Validation of the finite element model

3.1 Modal analysis

Modal analysis was conducted by the Block-Lanczos method to determine natural frequencies and mode shapes of the SMART 2013 structure. Structural mass (11.5 ton), additional mass on slabs (34.4 ton), and shaking table mass (25.0 ton) were counted in the modal analysis. To impose displacement boundary condition, we fixed the actuator positions in the shaking table. We obtained the first three natural frequencies of 6.26 Hz, 7.77 Hz, and 13.15 Hz, respectively, which were comparable to the natural frequencies determined by experiment in the SMART 2013 benchmark program (Richard and Charbonnel 2013). Table 4 shows the numerical and experimental values of the natural frequencies for the first three modes. Fig. 3 depicts the corresponding mode shapes. The first and second mode shapes represent primary flexure with respect to x and y axes, respectively, while the deformed shape of the third mode represents torsion of the structure with respect to z axis. It is noted that torsional behavior can be observed in all three modes due to the unsymmetrical geometry of the structure.

3.2 Linear time history analysis

Using the finite element model of the SMART 2013 RC structure, seismic analyses with respect to low-intensity ground motions were conducted. The ground motions were applied to the structure by a displacement control method at the actuator locations shown in Fig. 4(a). At the side of the shaking table, there are 4 actuators controlling the horizontal ground motion. There are additional 4 actuators at the bottom of the shaking table prescribing the vertical ground motion. Fig. 4(b) represents the location of sampling points on each floor.

Fig. 5 shows the low-intensity ground motions used for ‘run 6’ and ‘run 7’ in the SMART 2013 benchmark analysis. For the input ground motion of ‘run 6’, white noise is incorporated. The Peak

Table 4 Comparison of natural frequencies obtained by analysis and experiment

	Frequency (Hz)		
	Mode 1	Mode 2	Mode 3
Analysis	6.26	7.77	13.15
Experiment	6.28	7.86	16.50

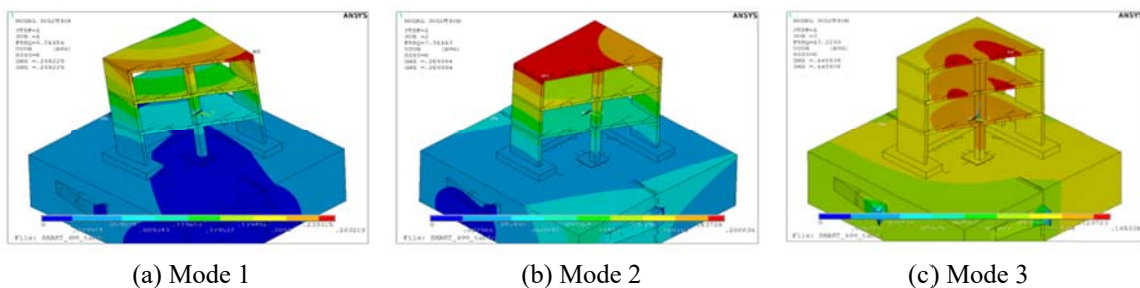


Fig. 3 Mode shapes of the SMART 2013 reinforced concrete structure

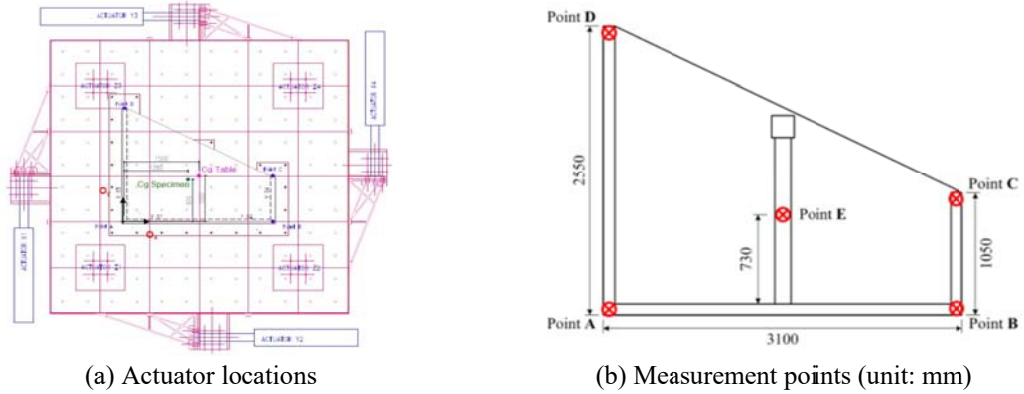
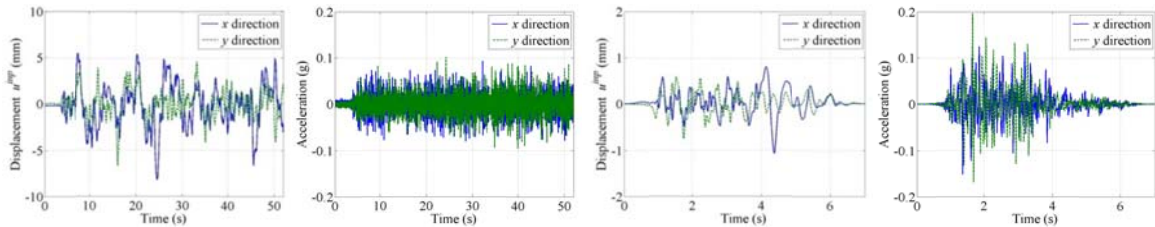


Fig. 4 Actuator locations and measurement points



(a) Displacement (run 6) (b) Acceleration (run 6) (c) Displacement (run 7) (d) Acceleration (run 7)
 Fig. 5 Low-intensity seismic loads for ‘run 6’ and ‘run 7’ of the SMART 2013 benchmark analysis

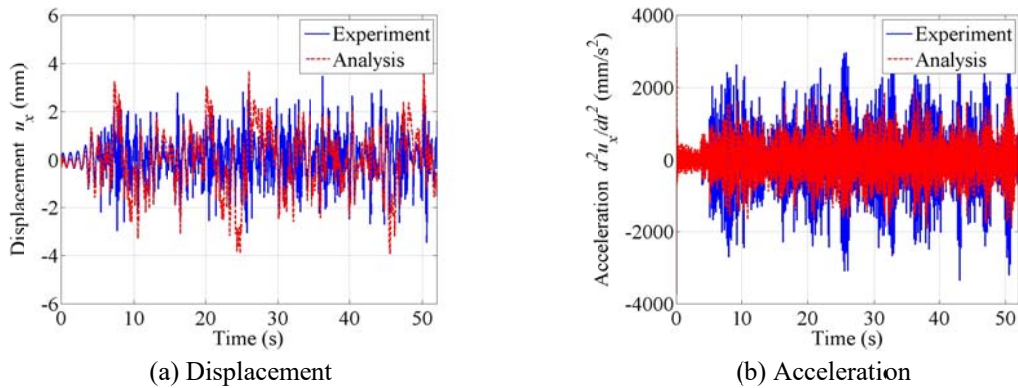


Fig. 6 Numerical and experimental responses in the x-direction at point D of the 3rd floor (run6)

Ground Acceleration (PGA) of the motions is about 0.1 g in both directions. Responses of the structure due to the low-intensity ground motions were computed without using nonlinear material models.

Figs. 6-12 show numerical and experimental responses of the SMART 2013 RC structure sampled at point D on the 3rd floor. On the whole, displacement and acceleration responses agree well with experiment results (Richard and Charbonnel 2013).

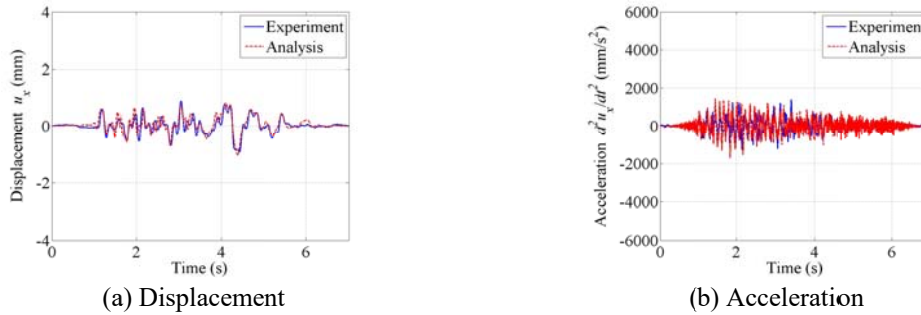


Fig. 7 Numerical and experimental responses in the x -direction at point D of the 1st floor (run7)

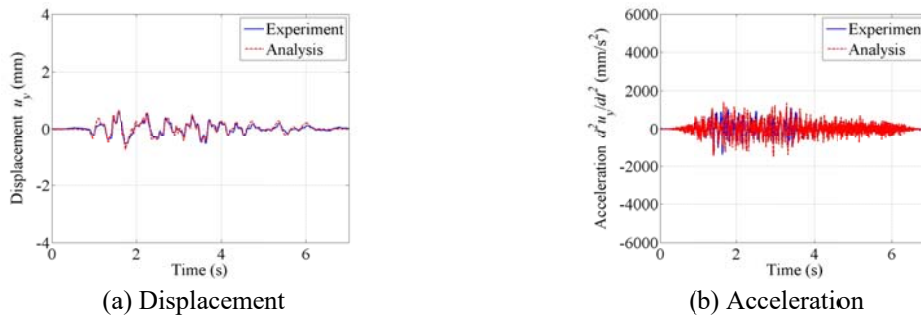


Fig. 8 Numerical and experimental responses in the y -direction at point D of the 1st floor (run7)

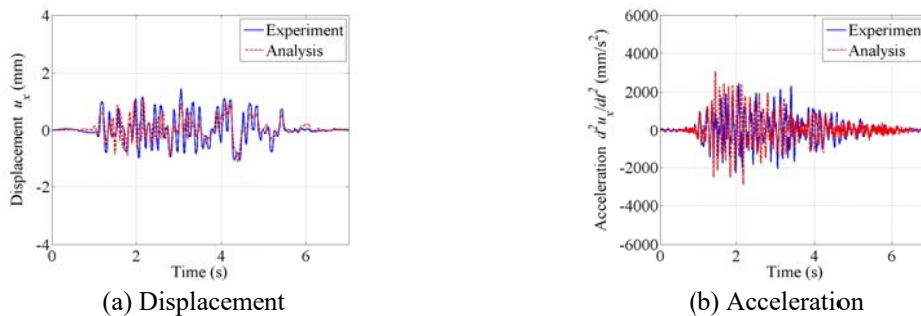


Fig. 9 Numerical and experimental responses in the x -direction at point D of the 2nd floor (run7)

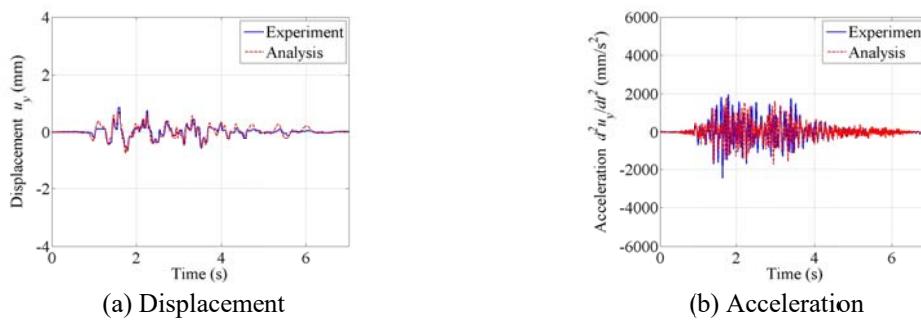


Fig. 10 Numerical and experimental responses in the y -direction at point D of the 2nd floor (run7)

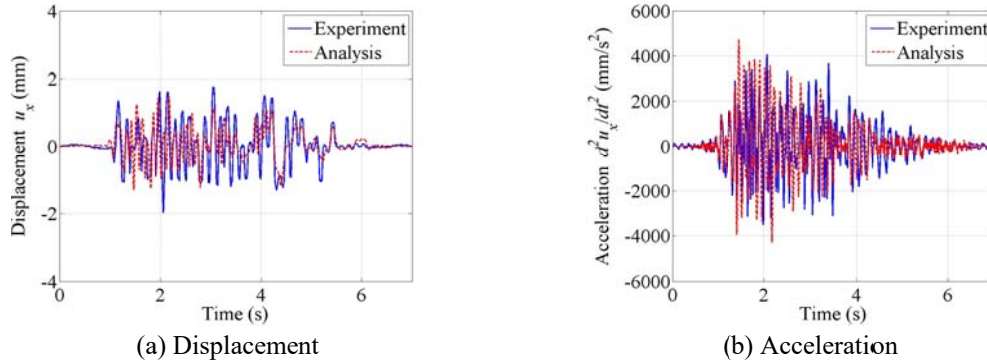


Fig. 11 Numerical and experimental responses in the x -direction at point D of the 3rd floor (run 7)

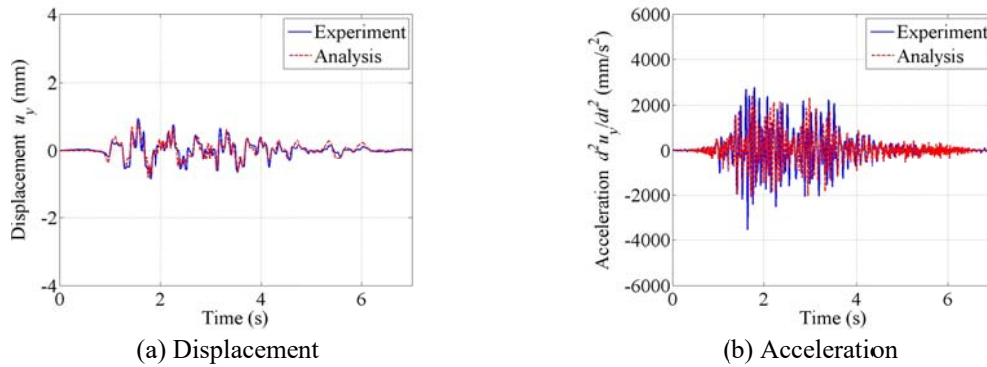


Fig. 12 Numerical and experimental responses in the y -direction at point D of the 3rd floor (run 7)

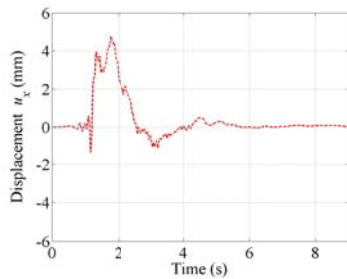
4. Nonlinear seismic analysis of the SMART 2013 RC structure

Nonlinear seismic analyses were performed for the SMART 2013 structure with high-intensity ground motions. The nonlinear seismic analyses comprise successive simulations of ‘run9’, ‘run11’, ‘run13’, ‘run17’, ‘run19’, ‘run21’, and ‘run23’ in the SMART 2013 benchmark program. Each case of simulations is described in Table 5. First of all, SMART 2013 RC structure was excited by synthetic design signal with the PGA of 0.2 g in both x and y directions at stage ‘run9’. The design signal is unscaled acceleration time history used for the design of the structure. The structure was then subjected to three seismic loads from ‘run11’ to ‘run17’, which were series of scaled Northridge earthquakes with the PGA up to 0.80 g and 0.42 g in x and y directions, respectively. Real Northridge earthquake was applied to the structure in ‘run19’, where PGAs were 1.78 g and 0.99 g in x and y directions, respectively. The structure was then excited by Northridge after-shocks in ‘run21’ and ‘run23’. The series of simulations were intended to estimate the seismic behavior of SMART 2013 RC structure with high-intensity ground motions close to real earthquake.

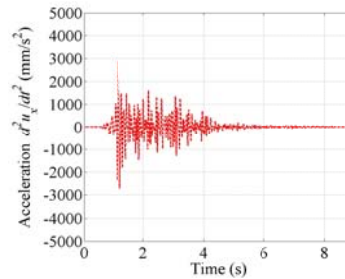
Figs. 13-19 present the displacement and acceleration responses of the structure in the x -direction at point D of the 3rd floor. The structural responses were largest for ‘run19’, where the maximum displacement is about 7.5 mm followed by residual deformation of about 2 mm.

Table 5 Sequence of earthquake loads for nonlinear seismic analysis

Run	PGA X (g)	PGA Y (g)	Percentage of the nominal signal (%)	Type
9	0.20	0.20	100	Unscaled design signal (nominal)
11	0.20	0.11	11	Scaled Northridge earthquake
13	0.40	0.21	22	Scaled Northridge earthquake
17	0.80	0.42	44	Scaled Northridge earthquake
19	1.78	0.99	100	Unscaled Northridge earthquake (nominal)
21	0.12	0.07	33	Scaled Northridge after-shock
23	0.37	0.31	100	Unscaled Northridge after-shock (nominal)

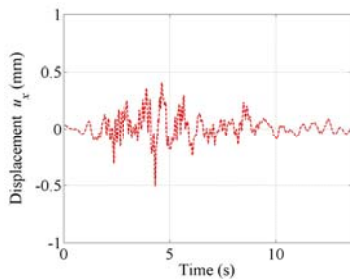


(a) Displacement in the x -direction

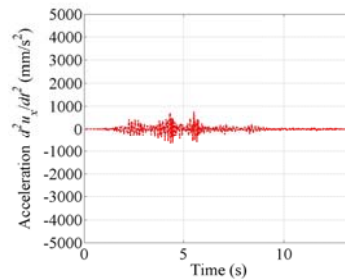


(b) Acceleration in the x -direction

Fig. 13 Response time histories at point D on the 3rd floor (Run 9)

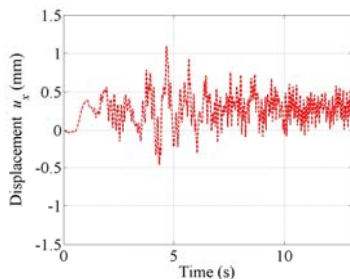


(a) Displacement in the x -direction

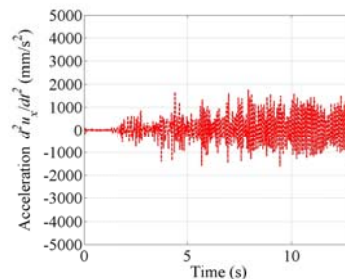


(b) Acceleration in the x -direction

Fig. 14 Response time histories at point D on the 3rd floor (Run 11)

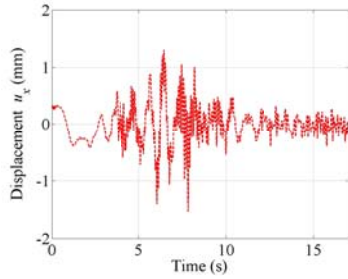


(a) Displacement in the x -direction

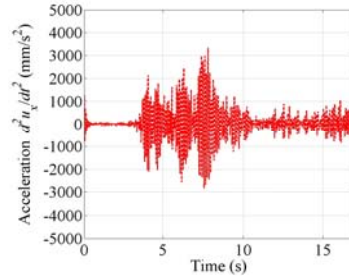


(b) Acceleration in the x -direction

Fig. 15 Response time histories at point D on the 3rd floor (Run 13)

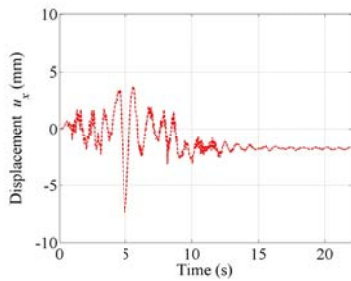


(a) Displacement in the x -direction

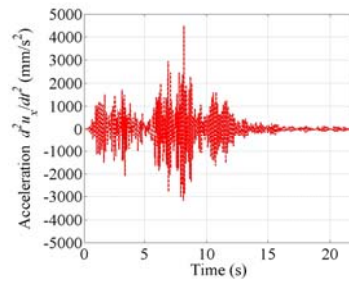


(b) Acceleration in the x -direction

Fig. 16 Response time histories at point D on the 3rd floor (Run 17)

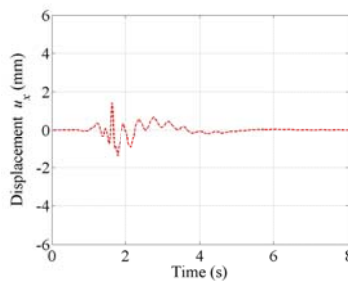


(a) Displacement in the x -direction

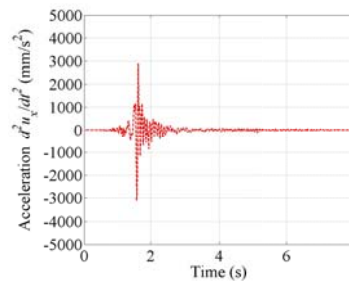


(b) Acceleration in the x -direction

Fig. 17 Response time histories at point D on the 3rd floor (Run 19)

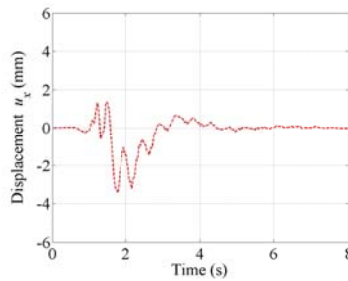


(a) Displacement in the x -direction

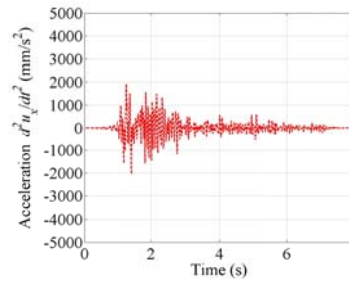


(b) Acceleration in the x -direction

Fig. 18 Response time histories at point D on the 3rd floor (Run 21)



(a) Displacement in the x -direction



(b) Acceleration in the x -direction

Fig. 19 Response time histories at point D on the 3rd floor (Run 23)

5. Seismic vulnerability analysis

Using the results of nonlinear seismic analyses, seismic fragility curves were constructed for the probabilistic damage assessment of the SMART 2013 RC structure. In this work, the maximum likelihood estimation method (Shinozuka *et al.* 2000, 2001, Hamburger *et al.* 2003, Kim and Shinozuka 2004, Kinali and Ellingwood 2007) was used for constructing fragility curves. Damage indicators and the thresholds for failure criteria of the SMART 2013 structure are as follows: maximum inter-story drift at point D of the 3rd floor, and frequency drop-off of the first and second modes. Damage levels are classified as light, controlled, and extended damages. The threshold for each damage is $h/400$, $h/200$, and $h/100$ ($h=1.2$ m denotes the story height) for the maximum inter-story drift, while the thresholds are 15%, 30%, and 50% for the frequency drop-off.

To construct fragility curves, a set of 100 input ground accelerations with various intensity and frequency contents were applied to the structure. The PGA of the ground motion ranges from 0.07 g to 2.51 g. In calculating the seismic response of the structure, soil-structure interaction effect was included by considering the stiffness and damping of the foundation system in swaying, pumping,

Table 6 Statistical parameters of the probability density functions

Property	Mean value	Coeff. of variation [%]
Tensile strength of floor	3.00 [MPa]	33
Equivalent rigid foundation stiffness in swaying	3.50×10^8 [N·m ⁻¹]	1
Equivalent rigid foundation stiffness in pumping	4.60×10^8 [N·m ⁻¹]	1
Equivalent rigid foundation stiffness in <i>x</i> -rocking	6.47×10^8 [N·m]	1
Equivalent rigid foundation stiffness in <i>y</i> -rocking	11.30×10^8 [N·m]	1
Equivalent rigid foundation damping in swaying	3.53×10^6 [N·s·m ⁻¹]	2
Equivalent rigid foundation damping in pumping	2.63×10^6 [N·s·m ⁻¹]	2
Equivalent rigid foundation damping in <i>x</i> -rocking	1.56×10^6 [N·s·m]	2
Equivalent rigid foundation damping in <i>y</i> -rocking	3.18×10^6 [N·s·m]	2
Structural damping ratio	3.00 [%]	20

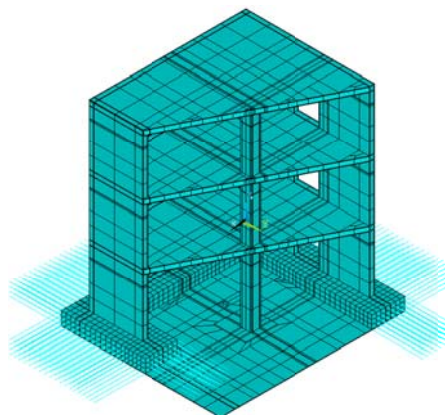


Fig. 20 Finite element model of the SMART 2013 RC structure with springs and dashpots at foundation

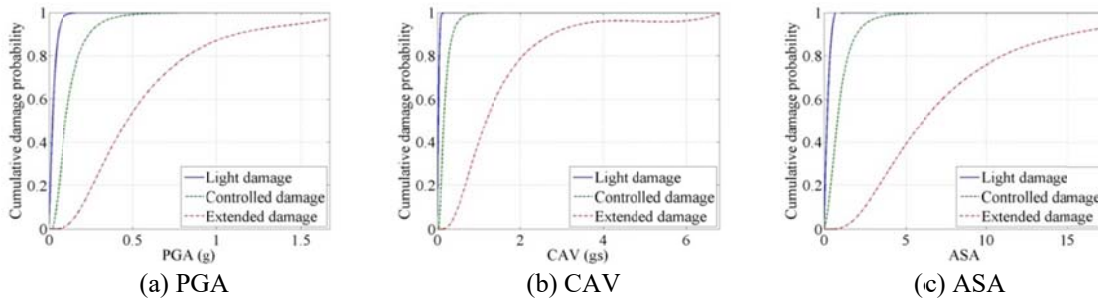


Fig. 21 Seismic fragility curves constructed by using the damage indicator of maximum inter-story drift in the x -direction

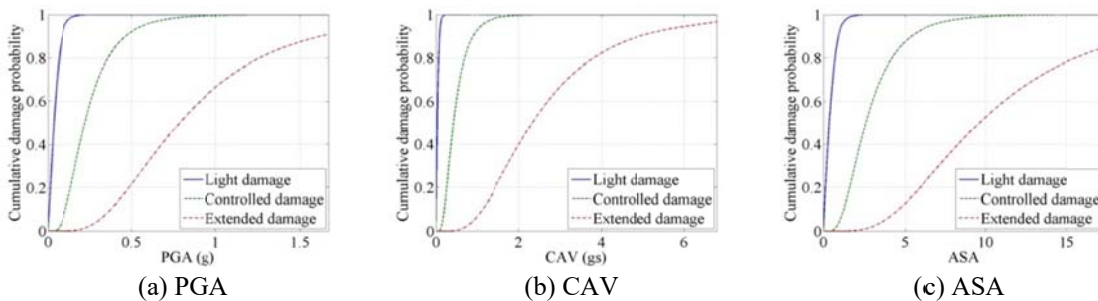


Fig. 22 Seismic fragility curves constructed by using the damage indicator of first frequency drop-off

and rocking motions (Zenter 2010, Zenter *et al.* 2011). The structural properties for the soil-structure interaction are presented in Table 6. Fig. 20 depicts the finite element model of the SMART 2013 structure with springs and dashpots at foundation.

Shown in Figs. 21 and 22 are seismic fragility curves of the structure for the damage indicators of maximum inter-story drift and frequency drop-off, respectively. The fragility was computed with respect to seismic intensity factors represented by PGA, cumulative absolute velocity (CAV), and structure-specific average spectral acceleration (ASA) (Campbell and Bozorgnia 2010, De Biasio *et al.* 2014). The fragility analyses showed that the SMART 2013 mock-up structure is likely to experience light damage for most of the input ground accelerations, and the probability of exceeding extended damage state is estimated to be over 90% for the ground motion with PGA level of 1.5 or higher.

6. Conclusions

This study presented the seismic performance evaluation of the SMART 2013 RC structure considering torsional effect and material nonlinearity. Nonlinear constitutive models for concrete and rebar were established and demonstrated by various local tests. The computed first three natural frequencies were 6.26 Hz, 7.77 Hz, and 13.15 Hz, respectively, and they were close to experimental results. In the linear time history analyses, displacement and acceleration responses at various sampling points showed good agreement with experimental results. Nonlinear time

history analyses were performed to evaluate the seismic behavior of the SMART 2013 structure for high-intensity ground motions. Finally, seismic fragility analyses were conducted for the damage assessment of the structure by the maximum likelihood method. The fragility analysis results showed that the probability of exceeding extended damage state would be over 90% for the ground motion with the PGA level of 1.5 or higher.

Acknowledgments

This research was supported by the Korea Institute of Nuclear Safety (grant No. 14-51), and by the Korea Institute of Energy Technology Evaluation and Planning (KETEP) and the Ministry of Trade, Industry & Energy (MOTIE) of the Republic of Korea (grant No. 20151520100990). The supports are greatly appreciated.

References

- Bisch, P. and Coin, A. (1994), "The CASSBA project", *Proceedings of the 10th European Conference on Earthquake Engineering*, Vienna, Austria.
- Bisch, P. and Coin, A. (1998), "The CAMUS research program", *Proceedings of the 11th European Conference on Earthquake Engineering*, Paris, France.
- Campbell, K. and Bozorgnia, Y. (2010), "A ground motion prediction equation for the horizontal component of Cumulative Absolute Velocity (CAV) based on the PEER-NGA strong motion database", *Earthq. Spectra*, **26**(3), 635-650.
- Crijanovschi, S., Richard, B., Chaudat, T. and Atanasiu, G.M. (2012), "Preliminary Numerical Analysis of a Reinforced Concrete Mock up: Effects of Thermal Breakers and Shaking Table", *Proceedings of the 15th World Conference on Earthquake Engineering*, Lisbon, Portugal.
- De Biasio, M., Grange, S., Dufour, F., Allain, F. and Petre-Lazar, I. (2014), "A simple and efficient intensity measure accounting for non-linear behavior of structure", *Earthq. Spectra*, **30**(4), 1403-1426.
- Hamburger, R.O., Foutch, D.A. and Cornell, C.A. (2003), "Translating research to practice: FEMA/SAC performance based design procedures", *Earthq. Spectra*, **19**(2), 255-267.
- Juster-Lermitte, S., Chaudat, T., Zenter, I. and Courtois, A. (2009), "Project SMART 2008", French Alternative Energies and Atomic Commission, Gif-sur-Yvette, France.
- Kachlakev, D. and Miller, T. (2001), "Finite element modeling of reinforced concrete structures strengthened with FRP laminates", Final report, Oregon Department of Transportation, OR, USA.
- Kim, S.H. and Shinozuka, M. (2004), "Development of fragility curves of bridge retrofitted by column jacketing", *Prob. Eng. Mech.*, **19**(1), 105-112.
- Kinali, K. and Ellingwood, B.R. (2007), "Seismic fragility assessment of steel frames for consequence based engineering: A case study for Memphis TN", *Eng. Struct.*, **29**(6), 1115-1127.
- Kwak, H.G. and Kim, D.Y. (2003), "Nonlinear finite element analysis of RC shear walls under cyclic loadings", *J. Comput. Struct. Eng. Inst. Korea*, **16**(4), 353-368.
- Kwak, H.G. and Kim, S.P. (2000), "Nonlinear analysis of RC beams under cyclic loading based on moment-curvature relationship", *J. Comput. Struct. Eng. Inst. Korea*, **13**(2), 245-256.
- Kwon, M. and Spacone, E. (2002), "Three-dimensional finite element analyses of reinforced concrete columns", *Comput. Struct.*, **80**(2), 199-212.
- Lee, H.P., Choun, Y.S. and Lee, S.J. (2007), "A study on the nonlinear analysis of containment building in Korea standard nuclear power plant", *J. Comput. Struct. Eng. Inst. Korea*, **20**(3), 353-364.
- Richard, B. and Charbonnel, P.E. (2013), "SMART 2013 International Benchmark Experimental data for stage #2", French Alternative Energies and Atomic Commission, Gif-sur-Yvette, France.

- Richard, B. and Chaudat, T. (2014), "Presentation of the SMART 2013 international benchmark", French Alternative Energies and Atomic Commission, Gif-sur-Yvette, France.
- Richard, B. and Ragueneau, F. (2012), "Nonlinear analysis of a reinforced concrete mock-up under seismic loading", *Proceedings of the 15th World Conference on Earthquake Engineering*, Lisbon, Portugal.
- Richard, B. and Ragueneau, F. (2013), "Continuum damage mechanics based model for quasi brittle materials subjected to cyclic loadings: Formulation, numerical implementation and applications", *Eng. Fracture Mech.*, **98**, 383-406.
- Richard, B., Fontan, M. and Mazars, J. (2014), "SMART 2013: overview, synthesis and lessons learnt from the International Benchmark", French Alternative Energies and Atomic Commission, Gif-sur-Yvette, France.
- Shekarbeigi, M. and Sharafi, H. (2015), "Constitutive model for concrete: An overview", *Curr. World Envir.*, **10**, 782-788.
- Shinozuka, M., Feng, M.Q., Kim, H.K. and Ueda, T. (2001), "Statistical analysis of fragility curves", Technical Report, Multidisciplinary Center for Earthquake Engineering Research, NY, USA.
- Shinozuka, M., Feng, M.Q., Lee, J. and Naganuma, T. (2000), "Statistical analysis of fragility curves", *J. Eng. Mech.*, **126**(12), 1224-1231.
- Wang, T. and Hsu, T. (2001), "Nonlinear finite element analysis of concrete structures using new constitutive models", *Comput. Struct.*, **79**(32), 2781-2791.
- Zenter, I. (2010), "Numerical computation of fragility curves for NPP equipment", *Nuclear Eng. Des.*, **240**(6), 1614-1621.
- Zenter, I., Humbert, N., Ravet, S. and Viallet, E. (2011), "Numerical methods for seismic fragility analysis of structures in nuclear industry: application to a reactor coolant system", *Georisk*, **5**(2), 99-109.